Heat transfer investigation in a three dimensional annulus made of laminated composite Aluminum/hexadecane and filled with porous media

دراسة انتقال الحرارة في محتوى حلقي ثلاثي الأبعاد مصنع من المادة المركبة Aluminum/hexadecane ومملوء بوسط مسامي

Prof. Dr.
Manal H. AL - Hafidh
University of Baghdad - college of Engineering

Abbreviations:

Cp: Specific heat at constant pressure (kJ/kg ^{o} C),

g: Acceleration due to gravity (m/s^2), kf: Thermal conductivity of the fluid (W/m K), ks: Thermal conductivity of the solid (W/m K), keff.: Effective thermal conductivity of the porous media (W/m K), K: Permeability (m^2), l: Cylinder length (m), L:Dimensionless cylinder length, Nu1: Local Nusselt number on the inner cylinder, Nu2: Local Nusselt number on the outer cylinder, Nuin: Average Nusselt number on the inner cylinder, Nuout: Average Nusselt number on the outer cylinder, p: Pressure (N/m2), q: Local heat flux (m), r: Radial coordinate (m), R: Dimensionless radial coordinate, Ra*: Modified Rayleigh number, Rr: Radius ratio, S: Fin pitch (m), T: Temperature (K), t: time (s), ur,uϕ, uz: velocity component in r,ϕ and z - direction (m/s), Ur, Uϕ, Uz: Dimensionless velocity component in R, ϕ and Z direction, x, y, z: Cartesian coordinate system (m), Z: Dimensionless axial coordinate, α: Thermal diffusivity (m^2/s), β: Volumetric thermal expansion coefficient (1/K), θ: Dimensionless temperature, ψr, $\psi\phi$, ψz: Vector potential component in R,ϕ and Z – direction**,** FAI**:** angular direction**.**

Key words:

Natural convection, inclined annulus, laminar flow, porous media, aluminum/hexadecane, phase change material.

Corresponding Author:

Abstract:-

Heat transfer by natural convection of air flow has been studied numerically in a three dimensional inclined annulus. Two cases are taken for the annulus material which is made of laminated composite materials. Aluminum/Hexadecane phase change material (PCM) is taken in the first case and pure hexadecane material in the second case for the purpose of comparison. The annulus enclosure is filled with porous media between two inclined concentric cylinders under steady state condition and constant wall temperature boundary condition. The parameters affected on the system are modified Rayleigh number ($10 \leq Ra^{*} \leq 1000$), radius ratio Rr (0.2, 0.3, 0.4 and 0.5) and the annulus inclination angle δ (0, 30, 45, 60 and 90). The results show a maximum heat transfer for horizontal Aluminum/Hexadecane annulus which increases with the increase of Ra^{*} and Rr. The maximum variance in heat transfer for the two materials is 65.4% for horizontal annulus with Rr=0.2 and $Ra^{*}=1000$. A correlation of Nu in terms of Ra^{*}, Rr and the annulus inclination angle δ has been developed for the two cases.

1. Introduction

Integrated PCM drywalls have high thermal capacity so they should be able to minimize the effect of large fluctuations in the external ambient temperature on the inside thermal environment of the building thereby shifting the heating and cooling loads to off-peak electricity periods.

Past studies have shown that PCM drywalls could be used to improve the thermal performances of building fabrics and help moderate the temperature variations through capturing a large proportion of the solar radiation incident on the walls or ceilings of such buildings

These materials are used in various designs to improve the characteristic of various constructions and reduce their weight. The properties of these materials and the problems of obtaining structural elements based upon them have been studied by researchers and engineers all over the world. The fields of composite applications are diversified (Freger et al., 2004). They include structural elements of flying vehicles, their casinos, wings, fuselages, tails and nose cones, jet engine stators, panels form various purposes, main rotors of helicopters, heat proofing components, construction elements such as panels, racks, shields, banking elements, etc.

(Darkwa and Zhou, 2011) summarized studies undertaken towards the development of a laminated composite phase change material (PCM) of drywall based on previous analytical work which used aluminum/hexadecane (PCM). The study also covered the selection and testing of various types of adhesive materials as a suitable bonding material. The effective thermal conductivity was measured and increased remarkably to 1.25 W/mK for aluminum/hexadecane as compared with 0.15 W/mK for pure hexadecane.

(Zhou and Zhao, 2011) presented an experimental study on heat transfer characteristics of PCMs embedded in open cell metal foams and expanded graphite, respectively. In this study the paraffin wax RT 27 and calcium chloride hexahydrate were employed as the heat storage media and the transient heat transfer behavior was measured. The results indicate that the addition of porous materials, either open-cell metal foams or expanded graphite, can enhance the heat transfer rate of PCMs. Especially for metal foams, the results showed that they can double the overall heat transfer rate during the melting processes.

Nagano proposed a system of direct heat exchange between granules including phase change material (PCM) and air. The PCM granules consist of granulated porous media with particle diameters of about 1- 3 mm and paraffin wax. At first, column experiments are performed with a packed bed of PCM granules. It is demonstrated that heat exchange flux between the PCM granules and air can be kept large and continuous during phase change.

(Mbaye and Bilgen, 2006) carried out a numerical simulation of transient heat transfer in a composite passive system consisting of air–phase change material–air, arranged as a rectangular enclosure.

The vertical boundaries of the enclosure are isothermal and the horizontal ones adiabatic. The enthalpy formulation with a fixed grid is used to study the process of phase change with liquid–solid interface zone controlled by natural convection. It is found that subcooling coefficient is the most important parameter influencing heat transfer, and for a given subcooling, there is an optimum phase change partition thickness

(Takahiro et al., 2013) described the development and performance of a direct-contact heat exchanger using erythritol as a phase change material (PCM) and heat transfer oil for accelerating heat storage. The effects of flow rate and inlet temperature were examined using three characteristic parameters.

Thermal energy storage applications such as solar hot water systems and off peak refrigeration systems are able to use PCMs to store heat or cooling. However, (Tay et al., 2012) presented the results of an experimental investigation carried out on a tube-in-tank design filled with PCM for cold storage applications. The PCMs used are salt hydrate with phase change temperature of 27 ^{o}C and water.

In the present research the natural convection heat transfer is investigated in an inclined annulus used as heat exchanger. Two cases are taken for the material of the annulus based on previous experimental work which used aluminum/hexadecane (PCM) of drywall. The ranges of the parameters affected on the study are modified Rayleigh number ($10 \leq Ra^{*} \leq 1000$), radius ratio Rr (0.2, 0.3, 0.4 and 0.5) and the annulus inclination angle δ (0, 30, 45, 60 and 90).

2. Objective of Research

In the present research the natural convection heat transfer is investigated in an inclined annulus used as heat exchanger. Two cases are taken for the material of the annulus based on previous experimental work which used aluminum/Hexadecane (PCM) of drywall and pure Hexadecane. The ranges of the parameters affected on the study are modified Rayleigh number ($10 \leq Ra^{*} \leq$

1000), radius ratio Rr (0.2, 0.3, 0.4 and 0.5) and the annulus inclination angle δ (0, 30, 45, 60 and 90).

3. Mathematical model

The schematic drawing of the geometry and the Cartesian coordinate system employed in solving the problem is shown in **Figure 3.1.**

In order to model the incompressible flow in the porous medium, the steady-state equations of the Darcy flow model, namely, the mass, the momentum (Darcy), the energy conservation laws and the Boussinesq's approximation are employed. These equations in vectorial notation are given by (Nield and Bejan 1999).

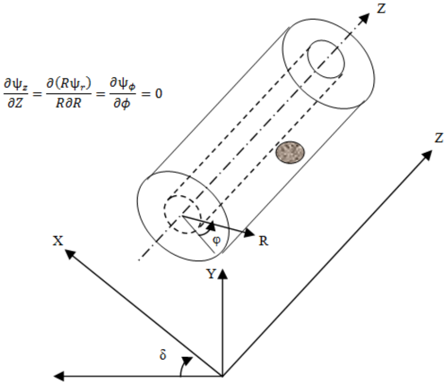

Figure 3.1: geometry and coordinates system

4. Governing equations

The conservation equations of mass, momentum and energy in steady state and the supplementary equation are:

$$\rho = \rho_2 \{1 - \beta(T - T_2)\} \qquad \text{Eq. 1}$$

Where:

$$\beta = \frac{1}{\rho}\frac{\partial \rho}{\partial T} \qquad \text{Eq. 2}$$

β Is the thermal coefficient of the volume expansion, this constant is evaluated at T_2 which is the temperature at the inner surface of the outer cylinder, ρ_2 is the density at T_2 and ρ is the density at T, (Fukuda et. al.1980). This technique is called Boussinesq's approximation.

4.1. Mass conservation

$$\frac{\partial u_r}{\partial r}+\frac{u_r}{r}+\frac{1}{r}\frac{\partial u_\phi}{\partial \phi}+\frac{\partial u_z}{\partial z}=0 \qquad \text{Eq. 3}$$

4.2. Momentum Equation

The most common model used for flow in the porous media is the Darcy flow model. Darcy’s law states that the volume average velocity through the porous material is proportional with the pressure gradient. In three dimensional flows, the Darcy’s model (Wang and Zhang 1990) is:

4.2.1. Momentum Equation in Radial Direction

$$u_r=\frac{K}{\mu_f}\left[-\frac{\partial p}{\partial r}-\rho\ g\ \cos\phi\right] \qquad \text{Eq. 4}$$

4.2.2. Momentum Equation In Angular Direction

$$u_\phi=\frac{K}{\mu_f}\left[-\frac{1}{r}\frac{\partial p}{\partial \phi}+\rho\ g\ \sin\phi\right] \qquad \text{Eq. 5}$$

4.2.3. Momentum Equation in Axial Direction

$$u_z=\frac{K}{\mu_f}\left[-\frac{\partial p}{\partial z}-\rho\ g\right] \qquad \text{Eq. 6}$$

4.2.4. Energy Equation

$$\frac{\partial(\rho\, C_pT)}{\partial t}+u_r\frac{\partial}{\partial r}(\rho\, C_pT)+\frac{u_\phi}{r}\frac{\partial}{\partial \phi}(\rho\, C_pT)+u_z\frac{\partial}{\partial z}(\rho\, C_pT)= \qquad \text{Eq. 7}$$

$$\frac{1}{r}\frac{\partial}{\partial r}\left\{r\frac{\partial(k\,T)}{\partial r}\right\}+\frac{1}{r^2}\frac{\partial^2(k\,T)}{\partial \phi^2}+\frac{\partial^2(k\,T)}{\partial z^2}+\mu\,\Phi$$

Φ is viscous dissipation function.

A vorticity vector Ω and a vector potential Ψ with its components (Aziz and Hellums 1967):

And a vector potential Ψ with its components:

$$\Psi = (\psi_r, \ \psi_\phi, \ \psi_z))$$

Defined by:

$$U = \alpha_{eff.} \ \nabla \ X \ \Psi \qquad \text{Eq. 8}$$

$$\nabla^2 \psi_r = \frac{1}{R}\frac{\partial U_z}{\partial \phi} - \frac{\partial U_\phi}{\partial Z} \qquad \text{Eq. 9}$$

$$\nabla^2 \psi_\phi = \frac{\partial U_r}{\partial Z} - \frac{\partial U_z}{\partial R} \qquad \text{Eq. 10}$$

$$\nabla^2 \psi_Z = \frac{1}{R}\frac{\partial (R U_\phi)}{\partial R} - \frac{1}{R}\frac{\partial U_r}{\partial \phi}$$

$$-\frac{\partial^2 \psi_\phi}{\partial Z^2} - \frac{\partial^2 \psi_\phi}{\partial R^2} - \frac{1}{R^2}\frac{\partial^2 \psi_\phi}{\partial \phi^2} - \frac{2}{R^2}\frac{\partial \psi_r}{\partial \phi} + \frac{\psi_\phi}{R^2} - \frac{1}{R}\frac{\partial \psi_\phi}{\partial R} \qquad \text{Eq. 11}$$

5. Normalization

For the present study the characteristic length is taken as r_2 to normalize the governing equations to the dimensionless form, the dimensionless magnitudes are defined as follow:

$$R = \frac{r}{r_2}, \ Z = \frac{z}{r_2}, \ U_r = \frac{u_r \ l}{\alpha_{eff}}, \ U_\phi = \frac{u_\phi \ l}{\alpha_{eff}} \ U_z = \frac{u_z \ l}{\alpha_{eff.}}, \ \theta = (T - T_2)/(T_1 - T_2)$$

$$P = \frac{p \ K \ l}{\alpha_{eff} \ \mu_f \ r_2}$$

$$Ra^* = g \ \beta \ K \ (T_1 - T_2) \ (r_2 - r_1)/\alpha_{eff.} \ \upsilon$$

Substitute these dimensionless magnitudes in the governing equations. Alternative expressions of equation (3) may be written in terms of $\psi_r, \ \psi_\phi \ and \ \psi_z \ as:$

$$U_r = \left(\frac{1}{R}\frac{\partial \psi_z}{\partial \phi} - \frac{\partial \psi_\phi}{\partial Z}\right) \qquad \text{Eq. 12}$$

$$U_\phi = \left(\frac{\partial \psi_r}{\partial Z} - \frac{\partial \psi_z}{\partial R}\right) \qquad \text{Eq. 13}$$

$$U_z = \frac{1}{R}\left\{\frac{\partial}{\partial R}\left(R\,\psi_\phi\right) - \frac{\partial \psi_r}{\partial \phi}\right\}$$ Eq. 14

Taking curl of momentum equations to eliminate pressure terms, the momentum equations will be:

$$Ra^*\ \frac{l}{(r_2 - r_1)}\left(\frac{1}{R}\frac{\partial \theta}{\partial \phi} + \sin\phi\ \frac{\partial \theta}{\partial Z}\right) =$$

$$-\frac{\partial^2 \psi_r}{\partial R^2} - \frac{1}{R^2}\frac{\partial\,(R\psi_r)}{\partial R} - \frac{2}{R}\frac{\partial\,\psi_r}{\partial R} - \frac{1}{R^2}\frac{\partial^2 \psi_r}{\partial \phi^2} - \frac{\partial^2 \psi_r}{\partial Z^2} - \frac{2}{R}\frac{\partial\,\psi_z}{\partial Z}$$ Eq. 15

$$Ra^*\ \frac{l}{(r_2 - r_1)}\ \left(\cos\phi\ \frac{\partial \theta}{\partial Z} - \frac{\partial \theta}{\partial R}\right) =$$

$$-\frac{\partial^2 \psi_\phi}{\partial Z^2} - \frac{\partial^2 \psi_\phi}{\partial R^2} - \frac{1}{R^2}\frac{\partial^2 \psi_\phi}{\partial \phi^2} - \frac{2}{R^2}\frac{\partial\,\psi_r}{\partial \phi} + \frac{\psi_\phi}{R^2} - \frac{1}{R}\frac{\partial\,\psi_\phi}{\partial R}$$ Eq. 16

$$-Ra^*\ \frac{l}{(r_2 - r_1)}\ \left(\frac{1}{R}\cos\phi\frac{\partial \theta}{\partial \phi} + \sin\phi\frac{\partial \theta}{\partial R}\right) =$$

$$-\frac{\partial^2 \psi_z}{\partial R^2} - \frac{1}{R}\frac{\partial\ \psi_z}{\partial\ R} - \frac{1}{R^2}\frac{\partial^2 \psi_z}{\partial\ \phi^2} - \frac{\partial^2 \psi_z}{\partial\ Z^2}$$ Eq. 17

The vector potential equation was obtained in the dimensionless form as.

$$\nabla^2 \psi_r = -\frac{\partial^2 \psi_r}{\partial R^2} - \frac{1}{R^2}\frac{\partial\,(R\ \psi_r)}{\partial R} - \frac{2}{R}\frac{\partial\,\psi_r}{\partial R} - \frac{1}{R^2}\frac{\partial^2 \psi_r}{\partial \phi^2} -$$ Eq. 18

$$\frac{\partial^2 \psi_r}{\partial Z^2} - \frac{2}{R}\frac{\partial\,\psi_z}{\partial Z}$$

$$\nabla^2 \psi_\phi = -\frac{\partial^2 \psi_\phi}{\partial Z^2} - \frac{\partial^2 \psi_\phi}{\partial R^2} - \frac{1}{R^2}\frac{\partial^2 \psi_\phi}{\partial \phi^2} - \frac{2}{R^2}\frac{\partial\,\psi_r}{\partial \phi} + \frac{\psi_\phi}{R^2} - \frac{1}{R}\frac{\partial\,\psi_\phi}{\partial R}$$ Eq. 19

$$\nabla^2 \psi_z = -\frac{\partial^2 \psi_z}{\partial R^2} - \frac{1}{R}\frac{\partial\,\psi_z}{\partial R} - \frac{1}{R^2}\frac{\partial^2 \psi_z}{\partial \phi^2} - \frac{\partial^2 \psi_z}{\partial Z^2}$$ Eq. 20

And the energy equation will be:

$$\left(\frac{1}{R}\frac{\partial\psi_z}{\partial\phi}-\frac{\partial\psi_\phi}{\partial Z}\right)\frac{\partial\theta}{\partial R}+\frac{1}{R}\left(\frac{\partial\psi_r}{\partial Z}-\frac{\partial\psi_z}{\partial R}\right)\frac{\partial\theta}{\partial\phi}+ \qquad \text{Eq. 21}$$

$$\left(\frac{\psi_\phi}{R}+\frac{\partial\psi_\phi}{\partial R}-\frac{1}{R}\frac{\partial\psi_r}{\partial\phi}\right)\frac{\partial\theta}{\partial Z}$$

$$=\frac{l}{r_1}\left[\frac{\partial^2\theta}{\partial R^2}+\frac{1}{R}\frac{\partial\theta}{\partial R}+\frac{1}{R^2}\frac{\partial^2\theta}{\partial\phi^2}+\frac{\partial^2\theta}{\partial Z^2}\right]$$

5.1. Dimensionless Hydraulic Boundary Conditions

For the vector potential field, the boundary conditions are given as.

$$\frac{1}{R}\frac{\partial}{\partial R}\left(R\,\psi_r\right)=\psi_\phi=\psi_z=0 \qquad at\ R=R_1,1$$

$$\psi_r=\frac{\partial\,\psi_\phi}{\partial\,\phi}=\psi_z=0 \qquad at\ \phi=0,\ \pi$$

$$\psi_r=\psi_\phi=\frac{\partial\ \psi_z}{\partial\ Z}=0 \qquad at\ Z=0,\ L$$

5.2. Dimensionless Thermal Boundary Conditions

For the temperature field, the dimensionless thermal boundary conditions are:

$$\theta=1 \qquad at\ R=R_1=r_1/r_2$$

$$\theta=0 \qquad at\ R=R_2=1$$

$$\frac{\partial\theta}{\partial\phi}=0 \qquad at\ \phi=0,\ \pi$$

$$\frac{\partial\theta}{\partial Z}=0 \qquad at\ Z=0,\ L$$

$$k_{eff}=\left(1-\varepsilon\right)\,k_s+\varepsilon\,k_f \quad (22)$$

Two cases are taken the material of the annulus. For the purpose of comparison pure hexadecane and composite Aluminum/hexadecane are taken with Polyvinyl acetate (PVA) material as a suitable bonding material. The dynamic viscosity of the (PVA) bonding material is 12000 kg/m s and has a thermal

conductivity of 0.3 W/m K. The effective thermal conductivity of Aluminum/hexadecane is 1.25 W/mK as compared with 0.15 W/mK for pure hexadecane (Darkwa and Zhou, 2011).

Aluminum/ Hexadecane **Pure Hexadecane**

Figure 5.1: Sample of the Aluminum/Hexadecane and pure Hexadecane composite materials

6. Computational technique

Eq. (15, 16, 17, 21) were transformed into the finite difference equations, where the upwind differential method in the left hand side of the energy eq.(21) and the centered – space differential method for the other terms were used, and solved by using (SOR) method**.** A computer program was built using MATLAB-7 program to meet the requirements of the problem.

The value of the vector potential ψ will be calculated at each node, in which the value of vector potential is unknown, the other node will appear in the right hand side of each equation. As an initial value of iteration, zero is chosen for the vector potential field, while a conduction solution is adopted for temperature field. The index (n) was used to represent the nth – approximation of temperature denoted by θ^n and substituted into the approximated equations, which were solved to obtain the nth approximation of vector potential ψ, then ψ was substituted into eq. (22) to obtain θ^{n+1}. A similar procedure is repeated until the prescribed convergence criterion given by inequality:

$$Max \left| \frac{\theta^{n+1} - \theta^{n}}{\theta^{n}} \right| \leq 10^{-8}$$ was established

It is clear that as the grid becomes finer, the convergence of the results becomes better. The number of grid points used was 21 grid points in the R – direction, 31 in the ϕ – direction and 301 in the Z – direction which seems reasonable and will be used in the present study.

6.1. Calculation of Local and Average Nusselt Number

Local Nusselt number is the dimensionless parameter indicative of the rate of energy convection from a surface and can be obtained as follows:

$$Nu = \frac{q(r_2 - r_1)}{k(T_1 - T_2)} \qquad \text{Eq. 23}$$

The local Nusselt number Nu_1 and Nu_2 on the inner and the outer cylinders are written in the form**:**

$$Nu_1 = -(1 - R_1) \left(\frac{\partial \theta}{\partial R} \right)_{R=R_1} \qquad \text{Eq. 24}$$

$$Nu_2 = -(1 - R_1) \left(\frac{\partial \theta}{\partial R} \right)_{R=1_1} \qquad \text{Eq. 25}$$

The average Nusselt number Nu_{in} and Nu_{out} on the inner and the outer cylinders are defined as:

$$Nu_{in} = -(1 - R_1) \frac{1}{\pi L} \int_0^L \int_0^\pi \left(\frac{\partial \theta}{\partial R} \right)_{R=R} d\phi \; dZ \qquad \text{Eq. 26}$$

$$Nu_{out} = -(1 - R_1) \frac{1}{\pi L} \int_0^L \int_0^\pi \left(\frac{\partial \theta}{\partial R} \right)_{R=1} d\phi \; dZ \qquad \text{Eq. 27}$$

7. Results and Discussion

7.1. Isotherms and Streamlines Field

The dimensionless temperature distribution within the enclosure is presented in a contour map form. One section was selected in the (Z-R) plane along the length of the annulus, and the other in the (R-ϕ) plane in of the annulus, in a manner allowed studying the temperature distribution within each plane.

The figures 7.1 & 7.2 show the isotherms and streamlines for Al/hexadecane for Ra^* =100 and 1000 respectively. In the figure 7.1 the symmetry of the temperature distribution for horizontal annulus is clear and the parallel lines indicating that the heat is transferred by conduction. Far away from the inner cylinder, the isothermal lines are deformed from their conductive pattern, and become curvilinear indicating that an ascending and descending convective flows occur. As Ra^* increase in the figure 7.2 isotherms shift towards the outer (cold) cylinder and a thicker cold layer under the surface of the inner cylinder with a high temperature field above the inner cylinder will be observed

More heat is transported upward, and a large difference of temperature is observed between the upper and lower parts of the annulus. The streamlines in the figure 7.1 take a bean form with low values in the core and high intensity in the boundaries. As Ra^* increase in the figure 7.2 the streamlines values decrease in the core and its intensity increase in the bottom of the annulus due to the increase in heat transfer.

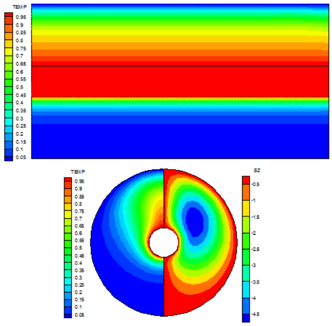

Figure 7.1: Isothermal and stream contours of Al/Hexadecane for $Ra^*=100$, $\delta=0$, $Rr=0.2$

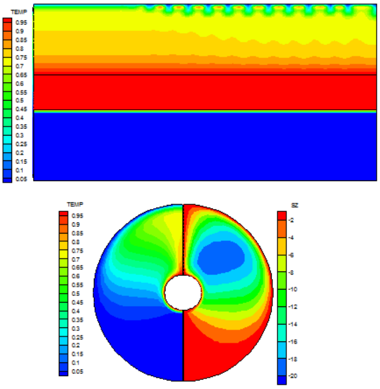

Figure 7.2: Isothermal and stream contours of Al/Hexadecane for Ra*=1000, δ=0, Rr=0.2

The figure 7.3 shows that as the inclination angle increase the symmetry of temperature distribution vanish and an increase in the region of temperature distribution clarify. The isotherms in the upper region shift towards the outer (cold) cylinder and the cold lower region will dwindle and a swell of the isothermal lines can observed when Ra* increase which implies a low Nu on the inner cylinder and a high Nu on the outer cylinder. Since this research was achieved for a steady state laminar region, thus the warm region at the top end when δ=90^o come to be as a concentric circles located at the center of the annulus and distributed between the hot and cold cylinders. When δ increases to 30^o, 45^o, 60^o and 90^o the center of the streamlines will be of negative values expand and fade away to the lower region.

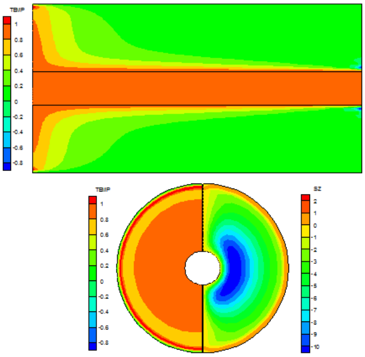

Figure 7.3: Isothermal and stream contours of Al/Hexadecane for Ra*=1000, δ=90, Rr=0.2

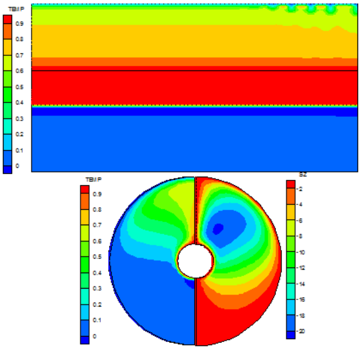

Figure 7.4: Isothermal and stream contours of pure hexadecane for $Ra^*=1000$, $\delta=0$, $Rr=0.2$

Comparing the figures 7.2 & 7.4 it is clear that because the pure hexadecane has a lower thermal conductivity than that of Al/Hexadecane, so the heat transfer is lesser and the temperature distribution show higher values than that in the figures 7.2 and so higher intensity of the streamlines will be observed.

Decreasing the gap of the annulus or in other word increasing the radius ratio to Rr (RI/RO) = 0.5 as shown in the figures 7.5 introduce an increase in temperature much faster near the hot wall and much slower near the cold wall. This further indicates that the sink temperature for the boundary layer on the hot wall reduces as the curvature effects increase. Also, for low radius ratios, the conduction in the core is very small for any given Ra^*.

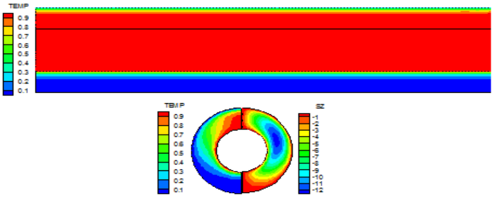

Figure 7.5: Isothermal and stream contours of pure hexadecane for $Ra^*=1000$, $\delta=0$, $Rr=0.5$

7.2. Average and Local Nusselt Numbers

The figures 7.6 & 7.7 show the variation of the average Nusselt number on the outer cold Al/Hexadecane cylinder with Ra^* for $\delta=0^o$,

45^o and 90^o respectively, at different radius ratios Rr. The figure illustrate an increase in Nu with Ra^* and Rr and the curves have a trend to coincide as Ra^* increase. As the inclination angle increase the average Nu decrease.

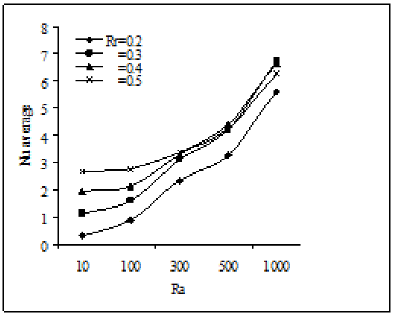

Figure 7.6: The variation of Nu with Ra* for Al/Hexadecane on the cold cylinder for δ=0 and different Rr

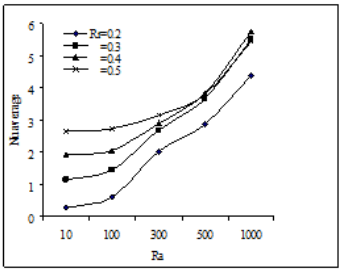

Figure 7.7: The variation of Nu with Ra* for Al/Hexadecane on the cold cylinder for δ=45o and different Rr

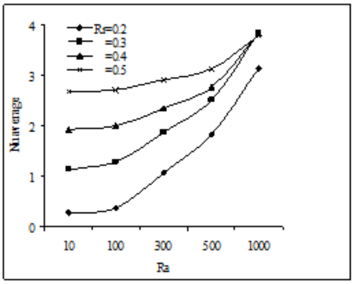

Figure 7.8: The variation of Nu with Ra* for Al/Hexadecane on the cold cylinder for δ=90o and different Rr

The figures 7.9 to 7.11 show the variation of the average Nusselt number on the outer cold pure Hexadecane cylinder with Ra^* for $\delta=0^o$, 45^o and 90^o respectively, at different radius ratios Rr. These figures illustrate the same behavior of the previous figures with a lesser values than that of the Al/Hexadecane due to the effect of thermal conductivity.

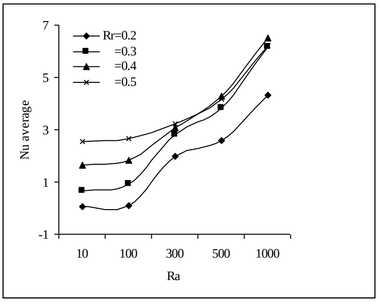

Figure 7.9: The variation of Nu with Ra* for pure Hexadecane on the cold cylinder for δ=0o and different Rr

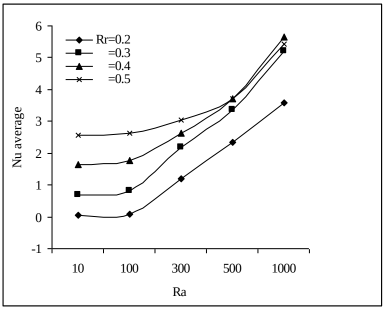

Figure 7.10: The variation of Nu with Ra* for pure Hexadecane on the cold cylinder for δ=45o and different Rr

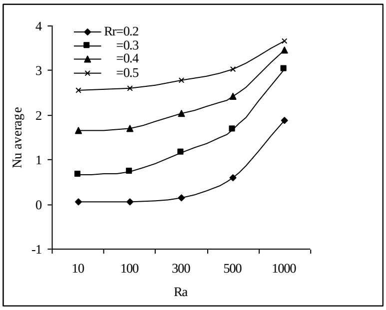

Figure 7.11: The variation of Nu with Ra* for pure Hexadecane on the cold cylinder for δ=90o and different Rr

The figures 7.12 and 7.13 show the variation of the average Nusselt number on the inner hot Al/Hexadecane cylinder with Ra^* for $\delta=0^o$ and 90^o respectively, at different radius ratios Rr. The figure illustrate an increase in Nu with the increase of Ra^* and the increase of Rr which means a decrease in the gap between the cylinders.

The figures 7.14 and 7.15 show the same trend for pure Hexadecane.

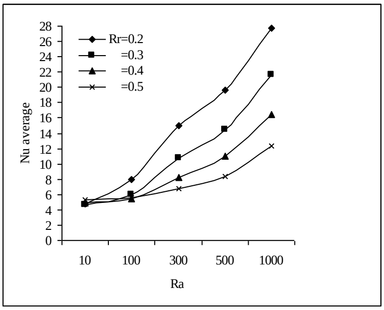

Figure 7.12: The variation of Nu with Ra* for Al/ Hexadecane on the hot cylinder for δ=0o and different Rr

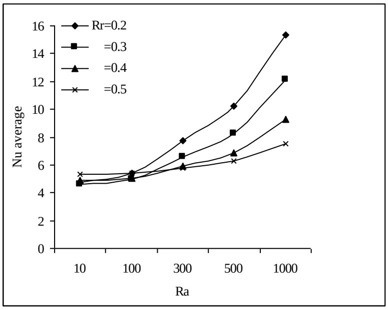

Figure 7.13: The variation of Nu with Ra* for Al/ Hexadecane on the hot cylinder for δ=90o and different Rr

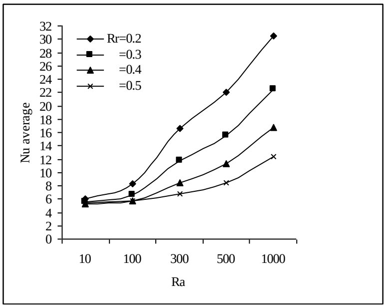

Figure 7.14: The variation of Nu with Ra* for pure Hexadecane on the hot cylinder for δ=0o and different Rr

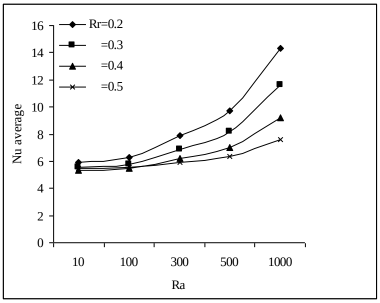

Figure 7.15: The variation of Nu with Ra* for pure Hexadecane on the hot cylinder for δ=90o and different Rr

The figures 7.16 and 7.17 show the variation of the average Nusselt number on the outer cold Al/Hexadecane cylinder with Ra* for Rr=0.3 and different δ. The figure illustrate an increase in Nu with Ra* and δ where δ=90^o means a horizontal annulus.

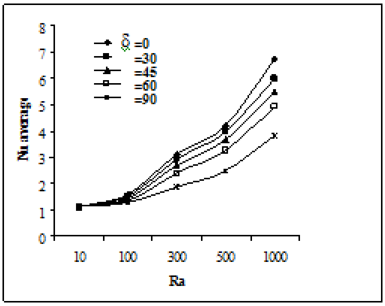

Figure 7.16: The variation of Nu with Ra* for Al/ Hexadecane on the cold cylinder for different δ and Rr=0.3

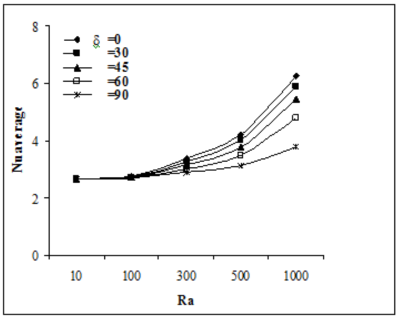

Figure 7.17: The variation of Nu with Ra* for Al/ Hexadecane on the cold cylinder for different δ and Rr=0.5

The variation of Nu with the radius ratio for different values of Ra* for δ=0^o and 90^o are shown in the figures 7.18 and 7.19 respectively. For low Ra*, Nu increase with Rr and as Ra* increase to 1000 Nu will be decrease after Rr become more than 0.3.

The figures 7.20 and 7.21 show the variation of the local Nusselt number along the length of the outer cold Al/Hexadecane cylinder with for Rr=0.2 and δ=0^o and 90^o respectively. The figure illustrate for δ=90^o (horizontal cylinder) a constant heat transfer along the cylinder length then an increase in the end of the cylinder rather than for δ=0^o (vertical cylinder) where Nu show a vacillation along the cylinder length.

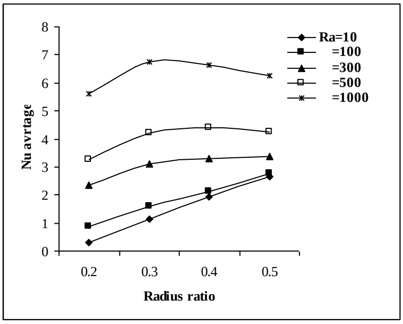

Figure 7.18: Variation of Nu average with the radius ratio Rr on the outer cold Al/Hexadecane cylinder for different Ra* and δ=0o

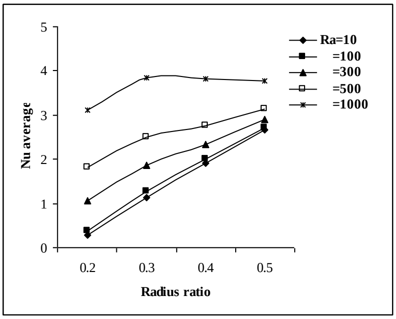

Figure 7.19: Variation of Nu average with the radius ratio Rr on the outer cold Al/Hexadecane cylinder for different Ra* and δ=90o

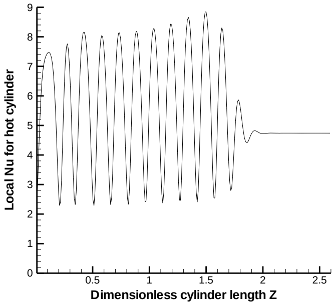

Figure 7.20: Variation of local Nu along the outer cold cylinder length for Al/Hexadecane at Rr=0.2 and δ=0o

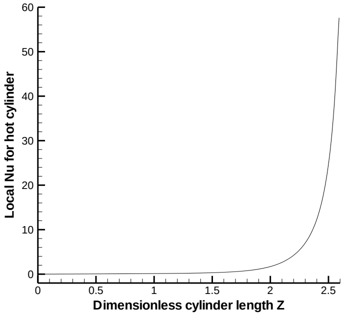

Figure 7.21: Variation of local Nu along the outer cold cylinder length for Al/Hexadecane at Rr=0.2 and δ=90o

When Rr increase to 0.5 the local Nu for $\delta=0^o$ show a high value in the starting point then take a constant value as shown in the figure 7.22.

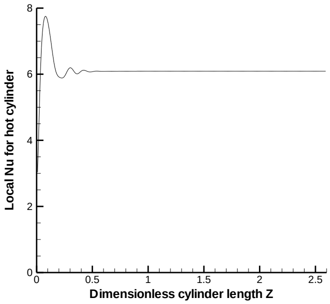

Figure 7.22: Variation of local Nu along the outer cold cylinder length for Al/Hexadecane at Rr=0.5 and δ=0o

Correlations were deduced from the numerical data for the outer cold cylinder which are given as:

For Al/Hexadecane:

$$Nu = \frac{1.515\ (R_a^*)^{0.31}\ (R_r)^{1.066}}{(\delta)^{1.079}}$$

For pure Hexadecane:

$$Nu = \frac{1.922\ (R_a^*)^{0.44}\ (Rr)^{2.208}}{(\delta)^{1.493}}$$

Conclusions:

The following major conclusions can be drawn from the study:

1- A 65.4% increase in the heat transfer is obtained when the Aluminum/Hexadecane used at $Ra^*=1000$ and $Rr=0.2$.

2- The average Nu number increases with the increase in modified Rayleigh number and Rr and decrease with increase in inclination angle.

3- For low Ra^*, Nu increase with Rr for the cold outer cylinder and as Ra^* increase to 1000 Nu will be decrease after Rr become more than 0.3.

الملخص:

تمت الدراسة العددية لانتقال الطاقة الحرارية بالحمل الطبيعي لجريان الهواء في محتوى حراري مائل ثلاثي الأبعاد. دُرست حالتين لمادة المحتوى التي صنعت من مواد مركبة مصفحة. في الحالة الأولى استخدمت المادة المركبة المتغيرة الطور Aluminum/Hexadecane وفي الحالة الثانية مادة الهكسادكين النقية pure hexadecane لغرض المقارنة. المحتوى الحراري مملوء بمادة مسامية بين أسطوانتين متمركزتين مائلتين تحت ظروف حالة الاستقرار ودرجة حرارة ثابتة للجدار. العوامل الاستدلالية المؤثرة هي عدد رالي المعدل $(10 \le Ra^* \le 1000)$ ونسبة

الأقطار Rr (0.2, 0.3, 0.4, 0.5) وزاوية ميلان المحتوى δ (0, 30, 45, 60 90). بينت النتائج أعلى انتقال في الطاقة الحرارية للمحتوى الأفقي المصنع من مادة Aluminum/Hexadecane والتي تزداد بزيادة Ra^* و Rr. أعلى فرق في انتقال الطاقة الحرارية بين المادتين 65.4% في حالة استخدام المحتوى الأفقي لمادة Aluminum/Hexadecane لعدد رالي $Ra^*=1000$ ولنسبة أقطار Rr=0.2. مثلت النتائج بمعادلات تجريبية تربط عدد نسلت بعدد رالي المعدّل ونسبة الأقطار وزاوية الميلان.

References:

- Hubert Jopek and Tomasz Strek, 2011, Optimization of the effective thermal conductivity of a Composite, http://www.intechopen.com/books/convection-andconduction-heat-transfer/optimization-of-theeffective-thermall conductivity-of-a-composite.

- Darkwa J., Zhou T., 2011 "Enhanced laminated composite phase change material for energy storage", Energy Conversion and Management 52, 810–815.

- Zhou D., Zhao C.Y., 2011,"Experimental investigations on heat transfer in phase change materials (PCMs) embedded in porous materials", Applied Thermal Engineering 31, 970-977.

- Nagano K., Takeda S., Mochida T., Shimakura K., 2004, Thermal characteristics of a direct heat exchange system between granules with phase change material and air, Applied Thermal Engineering 24, 2131–2144.

- Mbaye M., Bilgen E., 2006, "Natural convection in composite systems with phase change materials", Heat Mass Transfer 42, 636–644.

- Takahiro Nomura, Masakatsu Tsubota, Teppei Oya, Noriyuki Okinaka, Tomohiro Akiyama, 2013, "Heat storage in direct-contact heat exchanger with phase change material", Applied Thermal Engineering 50, 26-34.

- Tay N.H.S., Belusko M., Bruno F., 2012 "Experimental investigation of tubes in a phase change thermal energy storage system", Applied Energy 90, 288–297.

- Nield D. A. and Bejan A., “Convection in Porous Media”, Springer-Verlag, New York, 1999.
- Al- Hafidh Manal, Haithem H. Muhammad, Ban B. Jawad, 2014,"Effect of Angle of Rotation for Fiber Aligned in a Composite Material Wall of Inclined Enclosure on Heat Transfer", International Journal of Computer Applications, Volume 92 – No.12, 975 – 8887April.
- Wang Bu – Xuan and Zhang Xing, 1990, Natural Convection in Liquid Saturated Porous Media Between Concentric Inclined Cylinders, Int. J. Heat and Mass Transfer Vol. 33. No 5, 827-833.
- Aziz K. and Hellums J. D., 1967, Numerical Solution of the Three Dimensional Equations of Motion for Laminar Natural Convection, The Physics of Fluids, V0l. 10, No. 2, 314 – 324.